nature synthesis

Article

https://doi.org/10.1038/s44160-022-00235-w

Synthesis of covalent organic pillars as molecular nanotubes with precise length, diameter and chirality

Received: 25 September 2022

Accepted: 19 December 2022

Published online: 13 February 2023

Check for updates

Yaru Tian[1,2], Yunlong Guo[1], Xue Dong[1], Xintong Wan[2], Kuan-Heng Cheng[3], Rong Chang[1], Shunshun Li[1], Xiaoyu Cao[1], Yi-Tsu Chan[3] & Andrew C.-H. Sue[1]

The construction of nanotubes with well-defined structures, although synthetically challenging, offers the prospect of studying novel chemical reactions and transportation within confined spaces, as well as fabricating molecular devices and nanoporous materials. Here we report a discrete molecular nanotube, namely the covalent organic pillar **COP-1**, synthesized through a [2 + 5] imine condensation reaction involving two penta-aldehyde macrocycles and five phenylenediamine linkers. A pair of enantiomeric nanotubes, obtained in a quantitative and diastereoselective manner, were characterized and resolved readily. NMR spectroscopy, isothermal titration calorimetric and X-ray crystallographic studies revealed that the 2-nm-long and 4.7-Å-wide one-dimensional channel inside **COP-1** can accommodate α,ω-disubstituted *n*-alkyl chains with complementary lengths and electron density distributions. Furthermore, in a length-mismatched host–guest pair, we found that the nonamethylene dibromide thread not only displays a diminished binding constant in solution, but adapts an energetically unfavoured gauche conformation inside **COP-1** in the solid state.

Nanotubes[1–3], on account of their confined one-dimensional (1D) interior space, are fascinating nanoscale architectures with the potential for a plethora of applications, including molecular recognition and storage[4–7], catalysis[8,9], artificial channels for cross-membrane transportation[10–12], and nano-electronics and mechanical systems[13–15]. In addition to carbon nanotubes[16], the most renowned forms among this type of nanostructure, assorted tubular-shaped nano-assemblies with polymeric nature[17–20] have also been reported and studied extensively in the past decades. Nonetheless, their lack of structural precision, which renders it difficult to harness both their chemical and physical properties, has been a long-standing bottleneck hindering their further integration into complex molecular systems and functional materials. Atomically precise syntheses leading to discrete nanotubes[21–23] of uniform lengths and diameters, as well as one handedness when the target structures are chiral, are crucial for the full exploitation of the anisotropic interior 1D nanochannels. In recent years, although considerable advances in the syntheses of a range of novel macrocycles[24,25] and carbon nanobelts[26] have been made, single-molecule nanotubes with length/diameter ratios greater than unity are still few and far between in the literature.

One straightforward approach to building a discrete tube, be it macro-, micro or nanoscopic, is stacking (Fig. 1a) finite numbers of ring-shaped building blocks so that their cavity space can be extended along the axial direction. On the molecular level, assorted concave macrocyclic compounds (for example, cyclodextrins[27–29], cyclotriveratrylenes[30,31], resorcinarenes[32–35] and calixarenes[36–38]) have been employed in this regard to generate single open-ended cavitands and oligomeric tubular capsules with elongated cavities. Similarly,

[1]College of Chemistry and Chemical Engineering, Xiamen University, Xiamen, People's Republic of China. [2]Institute for Molecular Design and Synthesis, School of Pharmaceutical Science and Technology, Tianjin University, Tianjin, People's Republic of China. [3]Department of Chemistry, National Taiwan University, Taipei, Taiwan, Republic of China. e-mail: andrewsue@xmu.edu.cn

https://doi.org/10.1038/s44160-022-00235-w

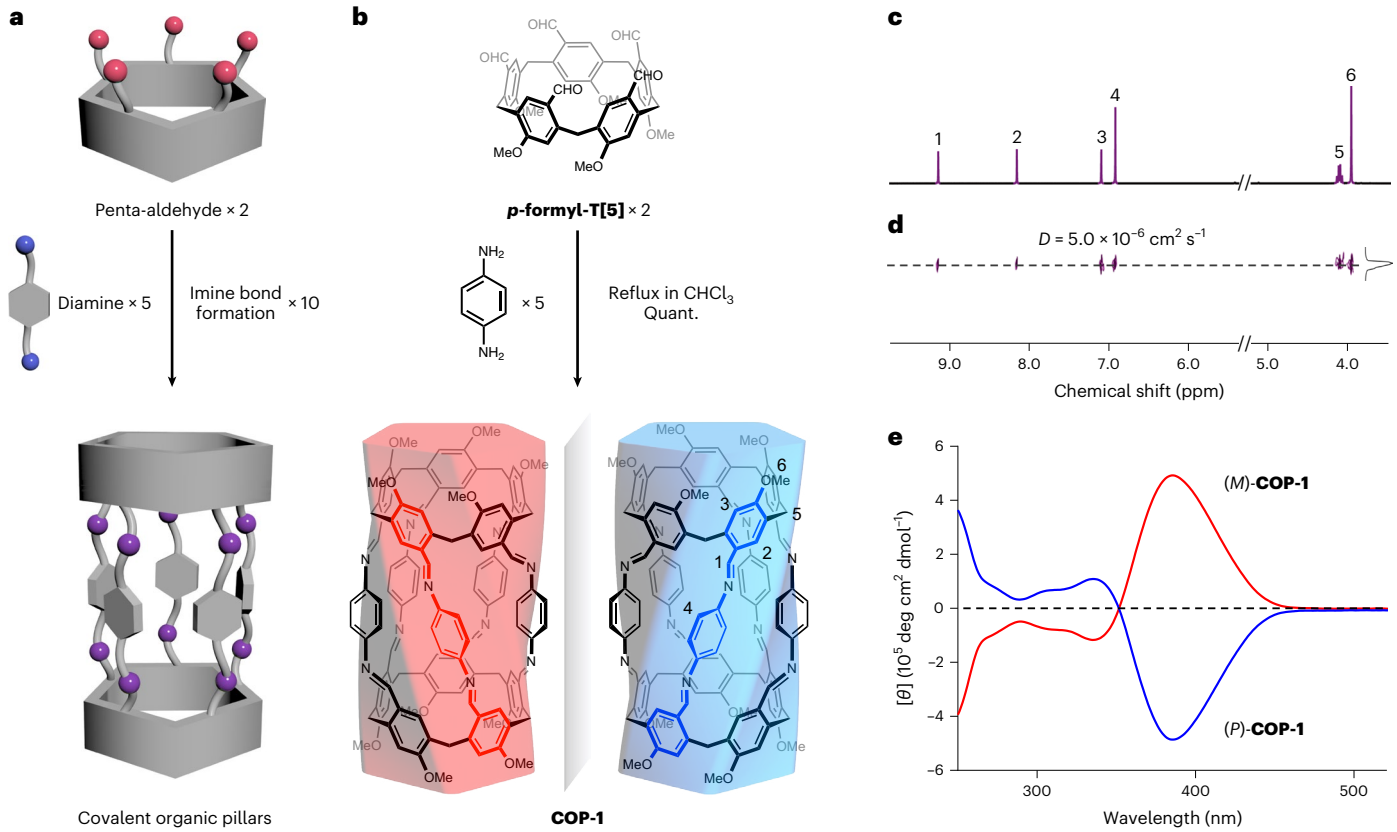

Fig. 1 | Design and synthesis of covalent organic pillars. a, Schematic of the molecular design of COPs. **b**, Synthetic scheme of **COP-1** involving [2 + 5] imine condensation of ***p*-formyl-T[5]** macrocycles and *p*-phenylenediamine linkers. Quant., quantitative yield. **c**,**d**, ^{1}H NMR (**c**) and DOSY spectra (600 MHz) (**d**) of **COP-1** recorded in CD_2Cl_2 at 298 K. **e**, ECD spectra of the (*M*)- and (*P*)-**COP-1** helical nanotubes recorded after chiral resolution.

pillararenes[39,40] and paracyclophane[41] derivatives, which can adopt straight pillar-like conformations, could serve naturally as ideal synthons for double open-ended uniform tubes.

To achieve controlled assembly of discrete pillararene superstructures, our research group has made strides in developing improved synthetic protocols for rim-differentiated pillararenes[42,43]. The capability to desymmetrize these macrocyclic scaffolds effectively, coupled with synthetic methodologies to derivatize[44] their distinct upper and lower rims with high selectivity, has already enabled[45–47] the syntheses of tubular pillararene oligomers through non-covalent weak interactions (for example, hydrogen bonds and metal coordination). Next, with the aim of synthesizing discrete covalent organic nanotubes in a similar fashion, we trimmed the alkoxy groups on one side of the rim-differentiated pillararene rings to produce[48] oligophenolic tiararenes, whose bare C–H functionalized rims allow for the execution of more derivatization schemes. By employing the Duff reaction, multiple aldehyde handles can be grafted onto the tiararene macrocycle for subsequent reactions with amine species to form dynamic covalent imine bonds, which have been used broadly in the construction of assorted covalent organic frameworks[49–52], molecular cages[53–55] and knots[56–58], and recently, both discrete and polymeric covalent organic nanotubes[20,23,59]. Following this molecular design strategy, herein we describe the successful construction and resolution of covalent organic pillars (**COP-1**)—a pair of 2-nm-long and 4.7-Å-wide chiral single-molecule nanotubes—as well as their stereochemistry, solid-state structures and host–guest properties.

Results and discussion

Synthesis of COP-1

The synthesis of **COP-1** was executed (Fig. 1b) by condensing the penta-aldehyde macrocycle ***p*-formyl-T[5]**[48] and *p*-phenylenediamine under reflux in $CHCl_3$ for 8 h. By virtue of the reversible nature of the dynamic covalent imine bonds, although numerous partially reacted intermediates were identified (Supplementary Fig. 10) over the course of the reaction, the targeted [2 + 5] **COP-1** with ten newly formed imine linkages was obtained (Supplementary Fig. 9) exclusively as the most thermodynamically stable species in a quantitative fashion. The resulting **COP-1** product is hardly soluble in most common laboratory solvents except chlorinated ones (for example, $CHCl_3$ and CH_2Cl_2, where moderate solubilities of 2.0 and 1.2 mg ml^{-1} were observed, respectively).

The ^{1}H NMR spectrum of **COP-1** shows (Fig. 1c) a relatively simple pattern because of the overall fivefold symmetry. Notable features of the spectrum include the emergence of an imine peak and the appearance of methylene bridge signals as a virtual quartet, both of which agree with the **COP-1** duplex formation. ^{1}H diffusion-ordered spectroscopy (DOSY) NMR confirmed (Fig. 1d) that all proton signals belong to a single species with a diffusion coefficient on the order of 10^{-6} cm^2 s^{-1}. The formation of the [2 + 5] **COP-1** product was also supported (Supplementary Fig. 3) by high-resolution mass spectrometry (HRMS) data.

Stereochemistry, chiral resolution and solid-state structure of COP-1

The inherently chiral ***p*-formyl-T[5]** precursor, in principle, undergoes rapid stereochemical inversion[60] similar to that of pillar[5]arenes. Such circumrotations shown by the aromatic units of the macrocycles are put to a halt in the **COP-1** duplex because of the presence of the imine covalent linkages. With the help of Pirkle's alcohol—a classic NMR chiral shift reagent—it was concluded (Supplementary Fig. 15) that the [2 + 5] condensation process between ***p*-formyl-T[5]** and *p*-phenylenediamine undergoes narcissistic chiral self-sorting, leading to the formation of a pair of **COP-1** enantiomers instead of a *meso* structure. By employing a preparative high-performance liquid chromatography (HPLC) system

https://doi.org/10.1038/s44160-022-00235-w

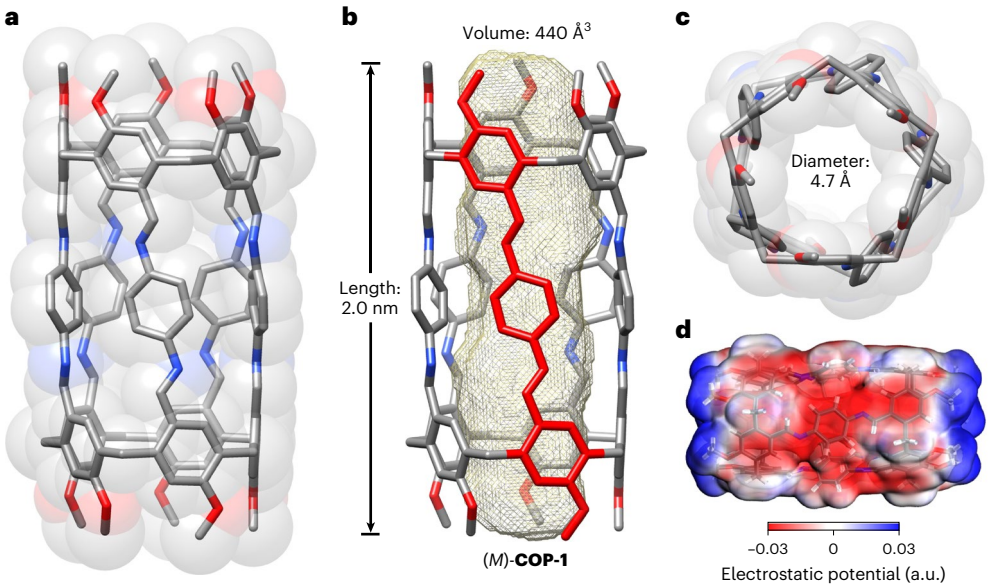

Fig. 2 | X-ray crystal structure of the COP-1 single-molecule nanotube. **a**, Fused stick/Corey-Pauling-Koltun (CPK) representation of (*M*)-**COP-1**. **b**, Side view of (*M*)-**COP-1** in stick representation, featuring the length and volume of the inner 1D channel. **c**, Top view of (*M*)-**COP-1** in fused stick/CPK representation, showing the inner diameter of the nanotube. **d**, Computational electrostatic potential map of **COP-1**. CH_2Cl_2 solvents and most hydrogen atoms are omitted for clarity. C, grey; O, red; N, blue; H, white; cavity space, gold. Part of (*M*)-**COP-1** is coloured in red to highlight the handedness. The channel volume was calculated using the VOIDOO program with a probe of 1.4 Å size. More information can be found in the Supplementary Information.

equipped with a chiral stationary phase, a racemic sample of **COP-1** was resolved (Fig. 1e and Supplementary Section 3) successfully into two enantiopure and stereostable fractions showing mirror image electronic circular dichroism (ECD) signatures.

The first fraction of **COP-1** showing a positive Cotton effect around 385 nm in the ECD spectrum was crystallized (space group $P2_12_12_1$; orthorhombic) by slow vapour diffusion of MeOH into a CH_2Cl_2 solution. X-ray crystallographic analysis confirmed (Fig. 2a) unambiguously the anticipated [2 + 5] nanotubular structure, which is manifested in the form of a hollow twisted pentagonal prism. The first resolved fraction was assigned (Supplementary Table 1) as the left-handed helical (*M*)-**COP-1** by X-ray diffraction analysis, and this stereochemical configuration was then validated (Supplementary Fig. 28) by computational methods. This enantiopure single-molecule nanotube features (Fig. 2b,c) an overall length of 2 nm between the methoxy tips on both ends, and a diameter of 4.7 Å defined by the macrocyclic aperture. The continuous 1D channel inside **COP-1**, which is occupied by four CH_2Cl_2 solvent molecules (omitted in Fig. 2; see Supplementary Fig. 18 for the complete [4•CH_2Cl_2⊂**COP-1**] inclusion complex), is estimated to have a void of ~440 $Å^3$.

Host–guest NMR investigations

The shape and size of **COP-1** suggest that, in addition to solvent molecules, this 2-nm-long nanotube could potentially host long linear guests. Nonetheless, no strong interactions between *n*-alkanes and the hollow channel of **COP-1** were observed (Supplementary Fig. 88) in the preliminary ^{1}H NMR spectroscopic studies, owing presumably to the lack of energetically favoured interactions between the non-polar paraffin guests and the inner wall of **COP-1**. Theoretical analyses of the electrostatic potential maps of **COP-1** (Fig. 2d and Supplementary Fig. 24) show that the channel surface is mostly electron rich except at the edges. Therefore, a series of *n*-alkyl chains with electron-withdrawing end groups (for example, *α*,*ω*-dibromoalkanes and *α*,*ω*-alkanediols) was chosen (Supplementary Fig. 25) as guest candidates by virtue of their complementarity to **COP-1** in terms of shape and electron density.

The host–guest complexations between **COP-1** and assorted *α*,*ω*-disubstituted *n*-alkanes in $CDCl_3$ were investigated (Fig. 3 and Supplementary Section 6) by NMR spectroscopic methods and HRMS. For the *α*,*ω*-dibromoalkane series, highly shielded proton signals below 0 ppm on the δ scale, corresponding to the encapsulated *n*-alkyl chains shielded by **COP-1**, appeared (Fig. 3 (left) and Supplementary Section 6.1) from samples containing 1,10-dibromodecane or longer *α*,*ω*-dibromoalkanes ($Br(CH_2)_nBr$ ($n \geq 10$); up to 1,20-dibromoicosane in our investigations; Supplementary Fig. 29). These high-field ^{1}H NMR peaks of bound guests, which display the same diffusion coefficients around 10^{-6} cm^2 s^{-1} as those of **COP-1** in the DOSY spectra, were assigned (Supplementary Section 6.1) based on the results of ^{1}H–^{1}H correlation spectroscopy. These observations indicate that the tubular cavity of **COP-1** shows effective binding with *α*,*ω*-dibromoalkanes longer than and equal to a certain critical length (*n*, 10).

In parallel, the investigations into the host–guest interactions between **COP-1** and *α*,*ω*-alkanediols led (Fig. 3 (right) and Supplementary Section 6.2) to similar results. The difference is that the proton signals of bound guests in the high-field spectral region could only be identified for [$HO(CH_2)_nOH$⊂**COP-1**] ($n \geq 12$) complexes containing 1,12-dodecanediol or longer *α*,*ω*-alkanediol threads (up to 1,22-docosanediol in our investigations). The critical length of the *α*,*ω*-alkanediol guests (*n*, 12) is two extra methylene units longer than that of the corresponding dibromides. Furthermore, it was found that the heteroatom is only required on one end of the *n*-alkyl chains, instead of both sides, to provide enough electron density complementarity. Clear high-field ^{1}H NMR proton peaks of encapsulated mono-substituted 1-bromoalkane and 1-alkanol guests inside **COP-1** were observed (Supplementary Section 6.3) from the [$Br(CH_2)_{n-1}CH_3$⊂**COP-1**] ($n \geq 12$; up to 1-bromooctadecane in our investigations) and [$HO(CH_2)_{n-1}CH_3$⊂**COP-1**] ($n \geq 13$; up to 1-tetradecanol in our investigations) complexes.

In the cases of 1,9-dibromononane and 1,11-undecanediol, which are both one methylene unit below the critical lengths in the respective dibromide and diol series, although no ^{1}H NMR peaks below 0 ppm occur (Fig. 3) on account of the shielding of the **COP-1** host, the broadened proton signals of the guest species in the spectra still suggest (Supplementary Figs. 29 and 62) the presence of host–guest interactions with intermediate exchange rates on the NMR time scale. In addition, the corresponding [$Br(CH_2)_9Br$⊂**COP-1**] and [$HO(CH_2)_{11}OH$⊂**COP-1**]

https://doi.org/10.1038/s44160-022-00235-w

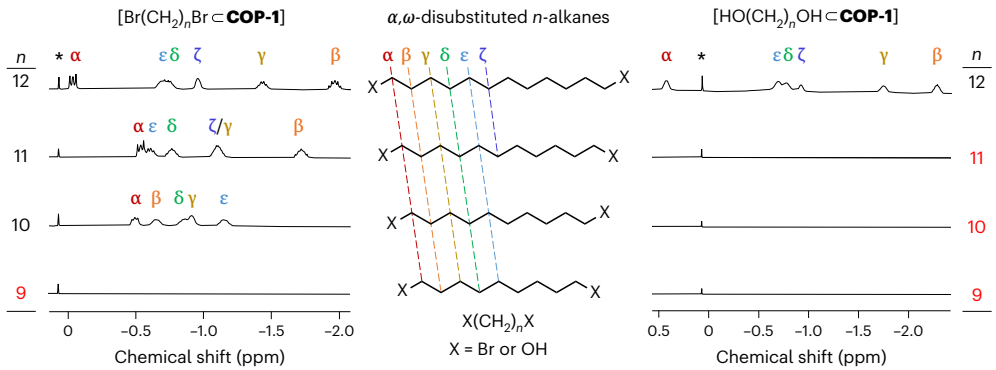

Fig. 3 | Host–guest interactions between COP-1 and *α*,*ω*-disubstituted *n*-alkanes. Stacked partial ^{1}H NMR (400 MHz) spectra of [Br(CH$_2$)$_n$Br⊂**COP-1**] (left) and [HO(CH$_2$)$_n$OH⊂**COP-1**] (right) inclusion complexes (*n*, 9–12) recorded in $CDCl_3$ at 298 K. Full ^{1}H NMR and ^{1}H–^{1}H correlation spectroscopy spectra used for detailed assignments of resonances in the high-field region can be found in the Supplementary Information. The asterisk denotes the NMR signal of silicone grease.

inclusion complexes were both identified (Supplementary Figs. 30 and 63) successfully in the HRMS spectra.

Further ^{1}H NMR titration experiments were conducted (Supplementary Figs. 59 and 84) between the **COP-1** host and 1,10-dibromodecane and 1,12-dodecanediol guests with the exact critical lengths required to form strong host–guest complexes. In these cases, free and bound guests could be identified clearly in the presence of excess guests, indicating that their threading–dethreading processes are within the slow exchange regime on the NMR time scale. When the amounts of the guests were less than one equivalent of **COP-1**, no NMR signal corresponding to the free guest could be observed at all in the spectra, and the chemical shifts of those bound guests remained unchanged regardless of their relative concentrations. These findings suggest that the association constants (K_a) of these host–guest systems are beyond the detection limit of the NMR titration method.

Binding constants between COP-1 and *α*,*ω*-disubstituted *n*-alkyl guests

To obtain accurate association constants and deeper insight into this host–guest system, the complexations of *α*,*ω*-disubstituted *n*-alkane guests over and below the critical lengths into the **COP-1** nanotube were probed (Supplementary Section 7) by isothermal titration calorimetry (ITC). The K_a values between the **COP-1** host and the 1,10-dibromodecane and 1,12-dodecanediol guests in $CHCl_3$ were found (Table 1) to be 1.19 and 2.36 × 10^5 M^{-1}, respectively, whereas the corresponding binding constants of the 1,11-dibromoundecane and 1,13-tridecanediol guests with one extra methylene group in the main chain are even higher (1.42 × 10^6 and 3.04 × 10^5 M^{-1}, respectively). These relatively strong binding affinities shown by **COP-1** towards these guests longer than and equal to the critical lengths corroborate with their tight binding mode and slow exchange dynamics observed in the NMR titration experiments. It is also noteworthy that these K_a values are at least three orders of magnitude larger than those between the *per*-methylated pillar[5]arene and the same guest species (Supplementary Figs. 104 and 106). The substantially stronger hosting ability displayed by the **COP-1** duplex than the individual macrocycle can be attributed to the pre-organization of the tubular structure, the enhanced stabilization provided by the extended inner surface and the rigid conformation without stereochemical inversion, which leads to less entropy loss upon guest binding.

In contrast, the host–guest pairs of **COP-1** and α,ω-disubstituted *n*-alkane guests shorter than the critical lengths show (Table 1) considerably diminished binding constants in $CHCl_3$. For example, the K_a values of the **COP-1** host with the 1,9-dibromononane and 1,11-undecanediol guests drop by one to two orders of magnitude to 2.41 × 10^3 and 3.45 × 10^4 M^{-1}, respectively. Further analyses of the isothermal titration calorimetry data reveal (Supplementary Tables 5 and 6) that these host–guest pairs have enthalpic gains comparable to those involving guests longer or equal to the critical lengths. At the same time, the more negative entropic terms observed, which lower the binding affinities between **COP-1** and these two shorter threads, can be attributed presumably to the greater configurational and/or conformational entropy loss suffered from the formations of mismatched host–guest complexes.

Table 1 | Binding constants between COP-1 and assorted *α*,*ω*-disubstituted *n*-alkane guests

	n	Guest	K_a (M^{-1})
Br(CH$_2$)$_n$Br	11	1,11-dibromoundecane[a]	(1.42±0.27)×10^6
	10	1,10-dibromodecane[a]	(1.19±0.06)×10^5
	9	1,9-dibromononane[a]	(2.41±0.19)×10^3
	8	1,8-dibromooctane[b]	(2.40±0.10)×10^3
HO(CH$_2$)$_n$OH	13	1,13-tridecanediol[a]	(3.04±0.02)×10^5
	12	1,12-dodecanediol[a]	(2.36±0.13)×10^5
	11	1,11-undecanediol[a]	(3.45±0.23)×10^4
	10	1,10-decanediol[b]	(9.43±0.22)×10^2

[a]ITC was performed in $CHCl_3$ at 298 K to obtain the K_a value. The data are expressed as means ± s.d. of triplicate experiments. [b]In the corresponding ITC experiments, no heat of interaction was measured. Instead, ^{1}H NMR titrations were performed in $CDCl_3$ at 298 K. The data were processed using BindFit (supramolecular.org) to obtain the K_a value and error (see Supplementary Information for more details).

To our surprise, shorter *α*,*ω*-disubstituted *n*-alkyl chains with two fewer methylene units below the critical length (for example, 1,8-dibromooctane and 1,10-dodecanediol) displayed no heat of interaction with **COP-1** in their respective ITC experiments, indicating that the complexation thermodynamic parameters become notably different for these shorter guests. Alternatively, by employing the ^{1}H NMR titration method, it was found (Table 1 and Supplementary Fig. 100) that the binding constant between **COP-1** and 1,8-dibromooctane is 2.40 × 10^3 M^{-1}, which is on a par with that corresponding to 1,9-dibromononane. In contrast, the 1,10-decanediol guest has (Table 1 and Supplementary Fig. 102) a two orders of magnitude lower K_a value (9.43 × 10^2 M^{-1}) towards **COP-1** compared with that of 1,11-undecanediol.

Overall, the binding constants shown by the **COP-1** nanotube vary over a wide range, spanning three orders of magnitude (10^6–10^3 and 10^5–10^2 M^{-1} for the dibromides and diols, respectively), for *α*,*ω*-disubstituted *n*-alkanes differing only by several methylene units.

https://doi.org/10.1038/s44160-022-00235-w

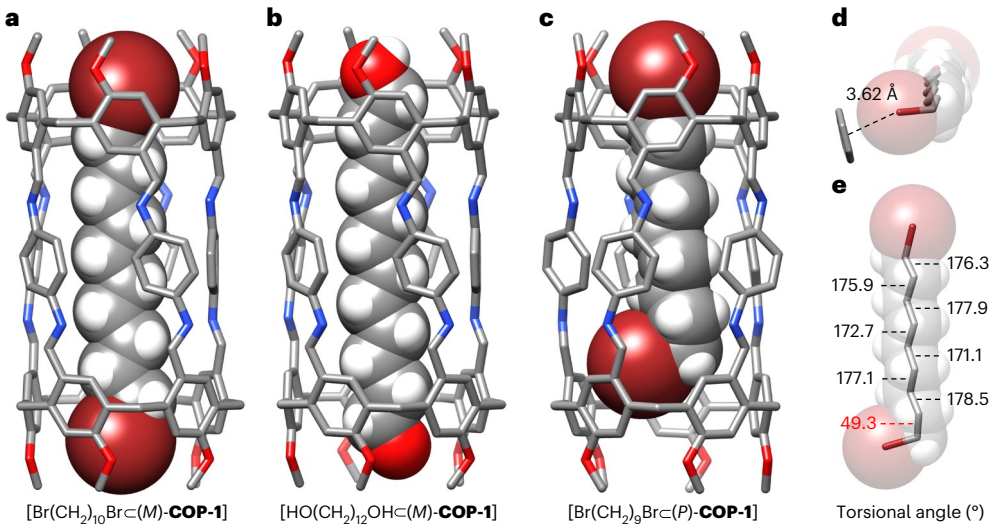

Fig. 4 | Threading of the COP-1 nanotube by *α*,*ω*-disubstituted *n*-alkanes. **a**–**c**, X-ray crystal structures of [Br(CH$_2$)$_{10}$Br⊂(*M*)-**COP-1**] (**a**), [HO(CH$_2$)$_{12}$OH⊂(*M*)-**COP-1**] (**b**) and [Br(CH$_2$)$_9$Br⊂(*P*)-**COP-1**] (**c**) inclusion complexes. The **COP-1** nanotubes and linear guests are shown in stick and CPK representations, respectively. **d**,**e**, Partial solid-state structures of the 1,9-dibromononane thread in fused stick/CPK representation, highlighting the C–Br···π interaction (**d**) and the torsional angles throughout the backbone (**e**). Hydrogens of **COP-1** are omitted for clarity. C, grey; O, red; N, blue; H, white; Br, brown.

High binding affinities ($K_a > 10^5$ M^{-1}) are exclusive for guest threads over and equal to the critical lengths, which presumably correspond to the overall size of the tubular channel of **COP-1**. This strong length dependence highlights the importance of host–guest complementarity in highly specific molecular recognition events.

Solid-state structures of COP-1 inclusion complexes

Finally, single crystals of the [Br(CH$_2$)$_{10}$Br⊂(*M*)-**COP-1**] and [HO(CH$_2$)$_{12}$OH⊂(*M*)-**COP-1**] inclusion complexes were obtained (both space group $P2_12_12_1$; orthorhombic) by slow evaporation of CH_2Cl_2 and $CHCl_3$ solutions containing (*M*)-**COP-1** and excess 1,10-dibromodecane and 1,12-dodecanediol, respectively. Their X-ray crystal structures substantiate (Fig. 4a,b and Supplementary Section 4) the threadings of the long linear decamethylene dibromide and dodecamethylene diol guests into the **COP-1** tubular channel. In these [2]pseudorotaxanes, the **COP-1** tubes adopt similar conformations with only minor variations in terms of void volume from that of the [4•CH_2Cl_2⊂**COP-1**] structure. The rigid and highly pre-organized **COP-1** tubular host allows both the 1,10-dibromodecane and 1,12-dodecanediol guests to adopt fully relaxed anti-periplanar conformations inside, showing torsional angles close to 180° throughout the backbone chains. The electron-withdrawing end groups, as anticipated, position in the centre of the electron-deficient opening areas at both ends of the tubular cavities. The X-ray crystallographic data also help to rationalize the different critical lengths shown by **COP-1** when interacting with the dibromide and diol guests. In the case of the [Br(CH$_2$)$_{10}$Br⊂**COP-1**] inclusion complex, the two large bromine atoms on both ends of the alkyl chain only require a spacer of ten methylene units to reach the electron-deficient edges of **COP-1**, whereas the 1,12-dodecanediol guest with smaller hydroxy groups needs two extra methylene units to be well stabilized inside the tubular channel of **COP-1** in the [HO(CH$_2$)$_{12}$OH⊂**COP-1**] complex.

In contrast, limited by the *n*-alkyl chain length, it is obvious that shorter *α*,*ω*-disubstituted *n*-alkane guests below the critical lengths cannot fully access the electron-deficient areas at both ends of the tube simultaneously, therefore resulting in weaker binding towards **COP-1** in solution. To further elucidate the exact mode of interactions between these length-mismatched host–guest systems, single crystals of the [Br(CH$_2$)$_9$Br⊂(*P*)-**COP-1**] complex were cured (space group $P2_12_12_1$; orthorhombic) by slowly evaporating a $CHCl_3$ solution containing (*P*)-**COP-1** and excess 1,9-dibromononene. In the solid-state structure (Fig. 4c and Supplementary Figs. 22 and 23), as one would expect, one of the bromine atoms of 1,9-dibromononene sits in the binding pocket at one side of the **COP-1** nanotube, whereas the rest of the carbon chain still adopts the extended zig-zag shape. The most striking feature of this X-ray crystal structure is that the remaining bromine, which cannot reach the tube opening, shows (Fig. 4d,e) an energetically unfavoured gauche torsional angle about the third adjacent carbon atom. The energy penalty of this distortion is compensated by a C–Br···π interaction (distance 3.62 Å) with an aromatic ring of the nearby macrocyclic unit, in addition to the stabilization provided by the interactions between the rest of guest and the inner wall of **COP-1**. This unusual geometry adapted by 1,9-dibromononene inside **COP-1** is reminiscent of the folding shown by guests with long *n*-alkyl chains inside cavitand-based molecular capsules[34]. Our unexpected observation represents a piece of rare crystallographic evidence for such contortion inside the confined space of a synthetic receptor.

Conclusion

In summary, we have successfully devised the synthesis of structurally precise single-molecule nanotubes by dimerizing rim-differentiated macrocycles with multiple covalent linkages. The application of reversible imine bonds, which marshals effective proofreading during the reaction process, avoids mismatch between the ring components and therefore leads to efficient formations of extended nanotubular structures. In particular, we employed penta-aldehyde tiara[5]arene-based macrocycles and ditopic *p*-phenylenediamine linkers as the building blocks for the construction of a pair of helical **COP-1** molecular nanotubes. We showcased that this highly pre-organized host, which possesses a 2-nm-long and 4.7-Å-wide 1D channel with an interior space of ~440 Å^3, displays specific recognition towards guests with complimentary size and electronic properties.

Our molecular design strategy for building COPs, applicable to [1$_n$] paracyclophane and pillar[*n*]arene derivatives, can also be potentially extended to a broad range of carbon nanorings and nanobelts. We hope that the development of the COPs will expedite the syntheses of discrete molecular nanotubes, or even pure carbon nanotubes, of a variety of sizes and functionalities. Such advancements will undoubtedly stimulate further explorations into molecular behaviours in confined

spaces from a fundamental science perspective and enable advanced technological applications in catalysis, biointerface and molecular nanotechnologies.

Methods

Synthesis of COP-1

***p*-formyl-T[5]** (20 mg; 0.027 mmol; 1.0 equiv.) and *p*-phenylenediamine (7.30 mg; 0.068 mmol; 2.5 equiv.) were dissolved in $CHCl_3$ (3 ml), then the reaction mixture was refluxed for 8 h to produce **COP-1** in a quantitative NMR yield. After the solvent was removed under reduced pressure, the crude product was washed with EtOAc (10 ml × 2) and MeOH (10 ml × 1) and dried under vacuum at 90 °C to afford **COP-1** as a yellow solid (24.8 mg; 94% isolated yield).

Chiral resolution of COP-1

HPLC separation was performed on a Shimadzu LC-16A instrument with a Daicel CHIRALPAK IE semi-preparative column (5 µm, ID 10 mm × L 250 mm). The racemic **COP-1** product (6.20 mg in 2 ml $CHCl_3$) was filtered with a syringe membrane filter before being injected into the HPLC system. In the mobile phase, the $CHCl_3$/MeOH ratio was 7:3, the flow rate was 2.0 ml min^{-1} and the detection wavelength was 300 nm. For one injection, 2.75 mg (*M*)-**COP-1** and 2.63 mg (*P*)-**COP-1** were collected. After resolution, the solubilities of enantiopure **COP-1** in $CHCl_3$ and CH_2Cl_2 increased to 4.0 and 1.8 mg ml^{-1}, respectively.

X-ray crystallography

Single-crystal X-ray diffraction data were collected on XtaLAB Synergy (Dualflex; HyPix) and XtaLAB Synergy R (DW system; HyPix) diffractometers using Cu Kα (λ = 1.54184 Å) micro-focus X-ray sources (PhotonJet (Cu) X-ray source). The raw data were collected and reduced using CrysAlisPro software. The structures were solved by ShelXT with intrinsic phasing and refined on F^2 using full-matrix least-squares methods, with ShelXL and Olex2 used as graphical user interfaces.

Computational methods

The electrostatic potential map was studied using a density functional theory calculation. All calculations were performed with the Gaussian 16 suite of computational programs. The B3LYP functional with the addition of the D3 version of Grimme's dispersion was employed to optimize all stationary points in the gas phase using 6-31G(d) basis sets for all atoms.

ITC

All titrations were conducted using a low-volume Affinity ITC (TA Instruments). Blank titrations in $CHCl_3$ were performed and subtracted from the corresponding titrations to attenuate the effect of dilution. The data fitting was executed using the NanoAnalyze program.

Data availability

The data that support the findings of this study are available in the Supplementary Information. Crystallographic data for the structure reported in this Article have been deposited at the Cambridge Crystallographic Data Centre under deposition numbers CCDC 2178245, 2178251, 2178252 and 2208259. Copies of the data can be obtained free of charge via https://www.ccdc.cam.ac.uk/structures/.

References

1. Bong, D. T., Clark, T. D., Granja, J. R. & Ghadiri, M. R. Self-assembling organic nanotubes. *Angew. Chem. Int. Ed.* **40**, 988–1011 (2001).
2. Mirzaei, S., Castro, E. & Sánchez, R. H. Conjugated molecular nanotubes. *Chem. Eur. J.* **27**, 8642–8655 (2021).
3. Shimizu, T., Ding, W. & Kameta, N. Soft-matter nanotubes: a platform for diverse functions and applications. *Chem. Rev.* **120**, 2347–2407 (2020).
4. Yamaguchi, T. et al. A 3.5-nm coordination nanotube. *J. Am. Chem. Soc.* **126**, 10818–10819 (2004).
5. Kameta, N., Minamikawa, H. & Masuda, M. Supramolecular organic nanotubes: how to utilize the inner nanospace and the outer space. *Soft Matter* **7**, 4539–4561 (2011).
6. Yazaki, K., Sei, Y., Akita, M. & Yoshizawa, M. A polyaromatic molecular tube that binds long hydrocarbons with high selectivity. *Nat. Commun.* **5**, 5179 (2014).
7. Altmann, P. J. & Pöthig, A. Pillarplexes: a metal–organic class of supramolecular hosts. *J. Am. Chem. Soc.* **138**, 13171–13174 (2016).
8. Pan, X. & Bao, X. The effects of confinement inside carbon nanotubes on catalysis. *Acc. Chem. Res.* **44**, 553–562 (2011).
9. Grommet, A. B., Feller, M. & Klajn, R. Chemical reactivity under nanoconfinement. *Nat. Nanotech.* **15**, 256–271 (2020).
10. Helse, A. J. et al. Highly conducting transmembrane pores formed by aromatic oligoamide macrocycles. *J. Am. Chem. Soc.* **130**, 15784–15785 (2008).
11. Chen, L. et al. Chiral selective transmembrane transport of amino acids through artificial channels. *J. Am. Chem. Soc.* **135**, 2152–2155 (2013).
12. Strilets, D. et al. Biomimetic approach for highly selective artificial water channels based on tubular pillar[5]arene dimers. *Angew. Chem. Int. Ed.* **59**, 23213–23219 (2020).
13. Collins, P. G., Zettl, A., Bando, H., Thess, A. & Smalley, R. E. Nanotube nanodevice. *Science* **278**, 100–102 (1997).
14. Kim, P. & Lieber, C. M. Nanotube nanotweezers. *Science* **286**, 2148–2150 (1999).
15. Avouris, P. Molecular electronics with carbon nanotubes. *Acc. Chem. Res.* **35**, 1026–1034 (2002).
16. Iijima, S. Helical microtubules of graphitic carbon. *Nature* **354**, 56–58 (1991).
17. Shimizu, T. Molecular self-assembly into one-dimensional nanotube architectures and exploitation of their functions. *Bull. Chem. Soc. Jpn* **81**, 1554–1566 (2008).
18. Chapman, R., Danial, M., Koh, M. L., Jolliffe, K. A. & Perrier, S. Design and properties of functional nanotubes from the self-assembly of cyclic peptide templates. *Chem. Soc. Rev.* **41**, 6023–6041 (2012).
19. Yashima, E. et al. Supramolecular helical systems: helical assemblies of small molecules, foldamers, and polymers with chiral amplification and their functions. *Chem. Rev.* **116**, 13752–13990 (2016).
20. Koner, K. et al. Porous covalent organic nanotubes and their assembly in loops and toroids. *Nat. Chem.* **14**, 507–514 (2022).
21. Neuhaus, P., Cnossen, A., Gong, J. Q., Herz, L. M. & Anderson, H. L. A molecular nanotube with three-dimensional π-conjugation. *Angew. Chem. Int. Ed.* **54**, 7344–7348 (2015).
22. Sun, Z. et al. Finite phenine nanotubes with periodic vacancy defects. *Science* **363**, 151–155 (2019).
23. Mao, L.-L. et al. Synthesis of finite molecular nanotubes by connecting axially functionalized macrocycles. *CCS Chem.* **4**, 3772–3780 (2022).
24. Liu, Z., Nalluri, S. K. M. & Stoddart, J. F. Surveying macrocyclic chemistry: from flexible crown ethers to rigid cyclophanes. *Chem. Soc. Rev.* **46**, 2459–2478 (2017).
25. Yang, L.-P., Wang, X., Yao, H. & Jiang, W. Naphthotubes: macrocyclic hosts with a biomimetic cavity feature. *Acc. Chem. Res.* **53**, 198–208 (2020).
26. Guo, Q. H., Qiu, Y., Wang, M. X. & Stoddart, J. F. Aromatic hydrocarbon belts. *Nat. Chem.* **13**, 402–419 (2021).
27. Harada, A., Li, J. & Kamachi, M. Synthesis of a tubular polymer from threaded cyclodextrins. *Nature* **364**, 516–518 (1993).
28. Wang, A., Li, W., Zhang, P. & Ling, C. C. Synthesis of a novel class of cyclodextrin-based nanotubes. *Org. Lett.* **13**, 3572–3575 (2011).

29. Kogame-Asahara, C. et al. A novel molecular tube fully modified at one end: selective inclusion of *cis*-unsaturated fatty acid esters. *Chem. Commun.* **56**, 1353–1356 (2020).
30. Brotin, T. & Dutasta, J.-P. Cryptophanes and their complexes—present and future. *Chem. Rev.* **109**, 88–130 (2009).
31. Henkelis, J. J. & Hardie, M. J. Controlling the assembly of cyclotriveratrylene-derived coordination cages. *Chem. Commun.* **51**, 11929–11943 (2015).
32. Quan, M. L. C. & Cram, D. J. Constrictive binding of large guests by a hemicarcerand containing four portals. *J. Am. Chem. Soc.* **113**, 2754–2755 (1991).
33. Heinz, T., Rudkevich, D. M. & Rebek, J. Jr. Pairwise selection of guests in a cylindrical molecular capsule of nanometre dimensions. Nature 394, 764–766 (1998).
34. Trembleau, L. & Rebek, J. Jr Helical conformation of alkanes in a hydrophobic cavitand. *Science* **301**, 1219–1220 (2003).
35. Kobayashi, K. & Yamanaka, M. Self-assembled capsules based on tetrafunctionalized calix[4]resorcinarene cavitands. *Chem. Soc. Rev.* **44**, 449–466 (2015).
36. Orr, G. W., Barbour, L. J. & Atwood, J. L. Controlling molecular self-organization: formation of nanometer-scale spheres and tubules. *Science* **285**, 1049–1052 (1999).
37. Kennedy, S. et al. Metal–organic calixarene nanotubes. *Angew. Chem. Int. Ed.* **49**, 4205–4208 (2010).
38. André, E. et al. A new, simple and versatile strategy for the synthesis of short segments of zigzag-type carbon nanotubes. *Chem. Eur. J.* **22**, 3105–3114 (2016).
39. Ogoshi, T., Kanai, S., Fujinami, S., Yamagishi, T.-A. & Nakamoto, Y. *para*-Bridged symmetrical pillar[5]arenes: their Lewis acid catalyzed synthesis and host–guest property. *J. Am. Chem. Soc.* **130**, 5022–5023 (2008).
40. Ogoshi, T., Yamagishi, T.-A. & Nakamoto, Y. Pillar-shaped macrocyclic hosts pillar[*n*]arenes: new key players for supramolecular chemistry. *Chem. Rev.* **116**, 7937–8002 (2016).
41. Takemura, H. [1$_n$]Paracyclophanes. *Curr. Org. Chem.* **13**, 1633–1653 (2009).
42. Guo, M. et al. Rim-differentiated C_5-symmetric tiara-pillar[5]arenes. *J. Am. Chem. Soc.* **140**, 74–77 (2018).
43. Chao, Y. et al. "Rim-differentiated" pillar[6]arenes. *Angew. Chem. Int. Ed.* **61**, e202204589 (2022).
44. Demay-Drouhard, P. et al. Functionalization at will of rim-differentiated pillar[5]arenes. *Org. Lett.* **21**, 3976–3980 (2019).
45. Fa, S., Sakata, Y., Akine, S. & Ogoshi, T. Non-covalent interactions enable the length-controlled generation of discrete tubes capable of guest exchange. *Angew. Chem. Int. Ed.* **59**, 9309–9313 (2020).
46. Fa, S. et al. Real-time chirality transfer monitoring from statistically random to discrete homochiral nanotubes. *Nat. Commun.* **13**, 7378 (2022).
47. Wan, X. et al. Twisted pentagonal prisms: Ag_nL_2 metal–organic pillars. *Chem* **8**, 2136–2147 (2022).
48. Yang, W. et al. Tiara[5]arenes: synthesis, solid-state conformational studies, host–guest properties, and application as nonporous adaptive crystals. *Angew. Chem. Int. Ed.* **59**, 3994–3999 (2020).
49. Côte, A. P. et al. Porous, crystalline, covalent organic frameworks. *Science* **310**, 1166–1170 (2005).
50. Liu, Y. et al. Weaving of organic threads into a crystalline covalent organic framework. *Science* **351**, 365–369 (2016).
51. Ma, T. et al. Single-crystal X-ray diffraction structures of covalent organic frameworks. *Science* **361**, 48–52 (2018).
52. Zhao, W. et al. Using sound to synthesize covalent organic frameworks in water. *Nat. Synth.* **1**, 87–95 (2021).
53. Tozawa, T. et al. Porous organic cages. *Nat. Mater.* **8**, 973–978 (2009).
54. Hassel, T. & Cooper, A. Porous organic cages: soluble, modular and molecular pores. *Nat. Rev. Mater.* **1**, 16053 (2016).
55. Hu, D., Zhang, J. & Liu, M. Recent advances in the applications of porous organic cage. *Chem. Commun.* **58**, 11333–11346 (2022).
56. Ayme, J.-F. et al. A synthetic molecular pentafoil knot. *Nat. Chem.* **4**, 15–20 (2012).
57. Lei, Y. et al. A trefoil knot self-templated through imination in water. *Nat. Commun.* **13**, 3557 (2022).
58. Wu, L. et al. Synthesis of contra-helical trefoil knots with mechanically tuneable spin-crossover properties. *Nat. Synth.* **2**, 17–25 (2023).
59. Shi, T.-H. et al. Discrete chiral organic nanotubes by stacking pillar[5]arenes using covalent linkages. *Cell Rep. Phys. Sci.* **3**, 101173 (2022).
60. Du, K. et al. Stereochemical inversion of rim-differentiated pillar[5]arene molecular swings. *J. Org. Chem.* **85**, 11368–11374 (2020).

Acknowledgements

This research work was financially supported by the Starry Night Science Fund of Zhejiang University's Shanghai Institute for Advanced Study (grant SN-ZJU-SIAS-006 to A.C.-H.S). We thank H. Cong (Technical Institute of Physics and Chemistry, Chinese Academy of Sciences), Z. Chen and L. Shi (both Zhejiang University) for insightful discussions and technical assistance and X. Zhang (Tianjin University) and all of the staff of the Analysis and Testing Center, College of Chemistry and Chemical Engineering, Xiamen University for assistance in various characterizations.

Author contributions

A.C.-H.S. conceptualized the study, validated the results, acquired funding and supervised the project. Y.T., Y.G., X.D., X.W., K.-H.C., R.C. and S.L. performed the investigations. Y.T., Y.G. and A.C.-H.S. developed the methodology. X.C., Y.-T.C. and A.C.-H.S. provided resources. A.C.-H.S. and Y.T. wrote the original draft of the manuscript. All authors reviewed and edited the manuscript.

Competing interests

The authors declare no competing interests.

Additional information

Supplementary information The online version contains supplementary material available at https://doi.org/10.1038/s44160-022-00235-w.

Correspondence and requests for materials should be addressed to Andrew C.-H. Sue.

Peer review information *Nature Synthesis* thanks Max von Delius, Alexander Pöthig and the other, anonymous, reviewer(s) for their contribution to the peer review of this work. Primary Handling Editor: Alison Stoddart, in collaboration with the *Nature Synthesis* team.